



RESEARCH ARTICLE

10.1029/2019JD031214

First 10 Months of TGF Observations by ASIM

Key Points:

- Simultaneous measurements of TGF by two spacecraft are presented
- Simultaneous measurements of TGF and Elve are not rare coincidence
- Imaging of TGF is presented
- The sequence of TGF and main optical lightning pulse is resolved
- TGFs observed from space have shorter duration than previously reported

Supporting Information:

- Supporting Information S1

Correspondence to:

N. Østgaard,
nikolai.ostgaard@uib.no

Citation:

Østgaard, N., Neubert, T., Reglero, V., Ullaland, K., Yang, S., Genov, G., et al. (2019). First 10 months of TGF observations by ASIM. *Journal of Geophysical Research: Atmospheres*, 124, 14,024–14,036. <https://doi.org/10.1029/2019JD031214>

Received 10 JUL 2019

Accepted 9 NOV 2019

Accepted article online 10 DEC 2019

Published online 19 DEC 2019

Author Contributions

Data curation: P. Kochkin, N. Lehtinen, D. Sarria, B. H. Qureshi, A. Solberg, C. Maiorana, K. Albrechtsen, C. Budtz-Jørgensen,

I. Kuvvetli, F. Christiansen, O. Chanrion, M. Heumesser, J. Navarro-Gonzalez, P. Connell, C. Eyles, H. Christian, S. Al-nussirat

Funding Acquisition: N. Østgaard, T. Neubert, V. Reglero

Methodology: N. Østgaard, V. Reglero,

M. Marisaldi, A. Mezentsev, O. Chanrion, M. Heumesser, P. Connell

N. Østgaard¹ , T. Neubert² , V. Reglero³, K. Ullaland¹ , S. Yang¹, G. Genov¹, M. Marisaldi¹ , A. Mezentsev¹ , P. Kochkin¹ , N. Lehtinen¹ , D. Sarria¹ , B. H. Qureshi¹, A. Solberg¹, C. Maiorana¹ , K. Albrechtsen¹ , C. Budtz-Jørgensen², I. Kuvvetli², F. Christiansen² , O. Chanrion² , M. Heumesser² , J. Navarro-Gonzalez³ , P. Connell³, C. Eyles³, H. Christian⁴, and S. Al-nussirat⁵

¹Birkeland Centre for Space Science, University of Bergen, Bergen, Norway, ²National Space Institute, Technical University of Denmark, Kongens Lyngby, Denmark, ³Image Processing Laboratory, University of Valencia, Valencia, Spain, ⁴Department of Atmospheric Science, University of Alabama in Huntsville, Huntsville, AL, USA, ⁵Department of Physics and Astronomy, Louisiana State University, Baton Rouge, LA, USA

Abstract The Atmosphere-Space Interactions Monitor (ASIM) was launched to the International Space Station on 2 April 2018. The ASIM payload consists of two main instruments, the Modular X-ray and Gamma-ray Sensor (MXGS) for imaging and spectral analysis of Terrestrial Gamma-ray Flashes (TGFs) and the Modular Multi-spectral Imaging Array for detection, imaging, and spectral analysis of Transient Luminous Events and lightning. ASIM is the first space mission designed for simultaneous observations of Transient Luminous Events, TGFs, and optical lightning. During the first 10 months of operation (2 June 2018 to 1 April 2019) the MXGS has observed 217 TGFs. In this paper we report several unprecedented measurements and new scientific results obtained by ASIM during this period: (1) simultaneous TGF observations by Fermi Gamma-ray Burst Monitor and ASIM MXGS revealing the very good detection capability of ASIM MXGS and showing substructures in the TGF, (2) TGFs and Elves produced during the same lightning flash and even simultaneously have been observed, (3) first imaging of TGFs giving a unique source location, (4) strong statistical support for TGFs being produced during the upward propagation of a leader just before a large current pulse heats up the channel and emits a strong optical pulse, and (5) the t_{50} duration of TGFs observed from space is shorter than previously reported.

1. Introduction

Terrestrial Gamma-ray Flashes (TGFs) discovered by Fishman et al. (1994) are flashes of gamma rays with energies up to 30–40 MeV (Briggs et al., 2010; Marisaldi et al., 2010, 2019), originating from thunderclouds, and their durations are from tens to more typically a few hundreds of microseconds (Connaughton et al., 2013; Gjesteland et al., 2010; Marisaldi et al., 2014). From spectral characteristics of TGFs observed from space (Dwyer & Smith, 2005) and associated radio measurements (Cummer et al., 2015) their production altitude has been found to be at 10–15 km produced in positive Intra Cloud (IC+) lightning bringing negative charge upward (Cummer et al., 2005; Stanley et al., 2006).

Combined with radio measurements it has been found that TGFs occur during the initial phase of lightning (Lu et al., 2010; Shao et al., 2010). This was also reported by Østgaard et al. (2013) based on the fortuitous coincidence of having two satellites passing less than 300 km apart, one detecting the optical signal from lightning and the other detecting the TGF. Simultaneous radio measurements from ground suggested the initiation of a leader about 4 ms before the TGF and that the main optical pulse was after the TGF. These results were revisited by Gjesteland et al. (2017) who also reported one more coincident observation of optical lightning and TGF and concluded that, with the temporal resolution of the optical data, they could not determine unambiguously the sequence of events, but only that the two signals were simultaneous to within ± 1.6 ms.

Several studies have reported that TGFs are associated with very large current pulses (>200 kA) that have been termed Energetic Intra-cloud Pulses (Cummer et al., 2014; Lyu et al., 2015). For a few cases it has been shown that a current pulse was observed simultaneously with the TGF and could well be from the TGF itself (Cummer et al., 2011; Pu et al., 2019). Whether this is true for all TGFs is an open question.

It has been suggested from theoretical considerations (Cummer et al., 2014; Lyu et al., 2015) and modeling (Liu et al., 2017) that a large current pulse observed by radio measurements simultaneously with TGFs

©2019. The Authors.

This is an open access article under the terms of the Creative Commons Attribution License, which permits use, distribution and reproduction in any medium, provided the original work is properly cited.

Software: V. Reglero, K. Ullaland, S. Yang, G. Genov, M. Marisaldi, A. Mezentsev, P. Kochkin, N. Lehtinen, D. Sarria, F. Christiansen, O. Chanrion, M. Heumesser, P. Connell, C. Eyles
Validation: N. Østgaard, V. Reglero, K. Ullaland, S. Yang, G. Genov, A. Mezentsev, P. Kochkin, N. Lehtinen, D. Sarria, B. H. Qureshi, A. Solberg, C. Maiorana, K. Albrechtsen, I. Kuvvetli, F. Christiansen, O. Chanrion, M. Heumesser, P. Connell, C. Eyles
Writing - Original Draft: N. Østgaard, V. Reglero, M. Marisaldi, A. Mezentsev, P. Kochkin, K. Albrechtsen, C. Eyles
Formal Analysis: N. Østgaard, V. Reglero, M. Marisaldi, A. Mezentsev, O. Chanrion, P. Connell
Investigation: N. Østgaard, T. Neubert, V. Reglero, K. Ullaland, S. Yang, G. Genov, M. Marisaldi, A. Mezentsev, P. Kochkin, N. Lehtinen, D. Sarria, B. H. Qureshi, A. Solberg, C. Maiorana, K. Albrechtsen, I. Kuvvetli, F. Christiansen, O. Chanrion, M. Heumesser, P. Connell, C. Eyles
Project Administration: N. Østgaard, T. Neubert, V. Reglero
Resources: N. Østgaard, T. Neubert, V. Reglero, K. Ullaland, S. Yang, G. Genov, B. H. Qureshi, A. Solberg, I. Kuvvetli, F. Christiansen, C. Eyles
Writing - review & editing: N. Østgaard

should also produce Elves, but this has not been observed before now. Atmosphere-Space Interactions Monitor (ASIM) is the first payload that has the ability to address this, and indeed, Neubert et al. (2019a), as the very first results from ASIM, reported the simultaneous detection of a TGF and an Elve, and that they were powered by the same lightning stroke. The TGF was observed at the end of a weak brightening interpreted as the propagation of an ascending leader in an IC+ lightning and had its onset $10\ \mu\text{s}$ ($\pm 5\ \mu\text{s}$) before the onset of a larger optical pulse. The TGF lasted for $80\ \mu\text{s}$. The optical pulse that followed peaked after $150\ \mu\text{s}$ and lasted for $\sim 1\ \text{ms}$. The pulse was interpreted as the optical signature of the current pulse that also produced the Elve.

It is now commonly accepted that TGFs are the results of relativistic electrons that produce X-rays and gamma rays through the bremsstrahlung process. Furthermore, these electrons have been accelerated in a very high electric field by the so-called runaway process (Wilson, 1925), and multiplied by orders of magnitude through a Relativistic Run-away Electron Avalanche (RREA) process (Gurevich et al., 1992). However, there are two main ideas to explain how the large number of gamma rays ($10^{17} - 10^{19}$) are produced. One (Babich et al., 2014, 2015; Moss et al., 2006; Chanrion & Neubert, 2010; Celestin & Pasko, 2011; Skeltved et al., 2017) considers the high electric field at the tip of a long conductive leader where the streamers in the streamer zone can produce 10^{12} electrons accelerated up to tens of keV and that these seed electrons are further accelerated and multiplied by RREA in the extended leader field to reach the necessary number of gamma photons. The other idea considers a feedback mechanism (Dwyer, 2008) where the gamma photons can backscatter or interact with neutrals to create pairs of electrons and positrons and that the gamma photons and positrons go back in the direction of the electric field to produce new seeds for avalanches (RREA). This mechanism does not need a lot of seed electrons, as the feedback can account for all the multiplication. The feedback mechanism could work both in a large uniform field and in the electric field ahead of a leader.

In this paper we present the first observations of TGFs by ASIM that was launched on 2 April 2018. Just during the first 10 months of observations, ASIM has provided several unprecedented measurements. In this paper we will report examples of these extraordinary findings, many of which will be analyzed in more detail in separate papers. However, already now we can draw conclusions from these observations that have important implications for TGF research.

2. Instruments and Data

The ASIM payload consists of two main instruments, the Modular X-ray and Gamma-ray Sensor (MXGS) and the Modular Multi-spectral Imaging Array (MMIA). The ASIM mission and the two instruments are documented in detail in the three papers by Neubert et al. (2019b), Østgaard et al. (2019), and Chanrion et al. (2019). Here we give a brief description of the mission and the instruments. As ASIM is mounted on the International Space Station (ISS), which is orbiting at about 400 km altitude with a 51.6° inclination, it will reach the latitudes where particles from the radiation belt and auroral particles precipitate in the upper atmosphere. While auroral observations and Lightning-induced Electron Precipitation are among the secondary objectives of ASIM, its main mission is to measure lightning, Transient Luminous Events (TLEs), and TGFs.

The MXGS has two detector layers for detecting X-rays and gamma rays. The MXGS Low-Energy Detector (LED) consists of pixelated (16,384 pixels) Cadmium-Zinc-Telluride detector crystals that detect photons with energies from 20 to 400 keV. Due to noise, the operational lower energy threshold is about 50 keV. The geometric area of the LED is $1,024\ \text{cm}^2$, and the effective detection area at 100 keV is $\sim 400\ \text{cm}^2$. A hopper-shaped collimator defines the $80^\circ \times 80^\circ$ fully coded field-of-view (FOV), while the total partially coded FOV is $138^\circ \times 138^\circ$, which covers the full Earth size from the ISS. A coded mask provides the imaging capability of the MXGS LED. The mask pattern is an 8×8 Perfect Binary Array of square-formed pixels, 54% open holes, and 46% closed by $46.2\ \text{mm} \times 46.2\ \text{mm} \times 1\ \text{mm}$ Tungsten plates. For more details about the coded mask structure we refer to Østgaard et al. (2019). The mask assembly is mounted over the aperture at the top of the hopper. The hopper walls are made of Aluminum (3 mm) and Tungsten (0.1 mm) and provide a good shielding up to 60 keV photons, which is the peak of Cosmic Diffuse X-ray Background. The mask is covered with a Kapton foil that stops electrons with energies up to 200 keV but allows photons down to 15 keV to enter the detector. From the penumbra pattern created by the flux of photons from a distant point source, their direction of arrival can be determined. The mask structure supports a weak radioactive source

(^{109}Cd), which is used for the in-flight calibration of the LED. Temporal resolution of the LED is about 1 μs with a dead time of about 1.4 μs . The LED only operates during nighttime.

The MXGS High-Energy Detector (HED) comprises 12 Bismuth-Germanium-Oxide (BGO) detector bars each coupled to a photomultiplier tube (PMT). The geometric detector area of HED is 900 cm^2 and is sensitive to photons with energies from 300 keV to >30 MeV. The effective detection area for HED is ~ 650 cm^2 at 1 MeV. The HED is mounted behind the LED and effectively shields the LED against radiation coming through the rear of the assembly. Three weak ^{22}Na radioactive sources are mounted in between the Cadmium-Zinc-Telluride detector plane and the BGO array. These sources are used to perform in-flight calibration of the BGO detectors. The FOV of the HED is 4π , and it is sensitive to bright TGFs up to at least 800 km from subsatellite point. Temporal resolution of the HED is 28.7 ns with a dead time of about 550 ns for detection by the same PMT/BGO detector module. There is no effective dead time for detection by a different detector module. The HED operates during day and night but is switched off during passage through the South Atlantic Anomaly, in order to protect the PMTs from aging and degradation due to high particle fluxes.

The MMIA includes two cameras imaging in 337.0 and 777.4 nm, at up to 12 frames per second, and three high-speed photometers at 337.0 nm (bandwidth 5 nm), 180–240 nm, and 777.4 nm (bandwidth 4 nm) with a 100 kHz sampling rate. The 777.4 nm emissions are from atomic oxygen and used for detecting lightning. As emissions in the Lyman-Birge-Hofmann UV band (180–240 nm) will be absorbed by molecular oxygen this band will be most sensitive to high altitude phenomena such as TLEs. The 337.0 nm (N_2^2P) will be most sensitive to lightning but will also see weak signals from TLEs. The FOV of the cameras and the two photometers are square with 80° diagonal, while the UV photometer FOV is circular with 80° full cone angle. The MMIA only operates during night time.

The two instruments, MMIA and MXGS, constitute a triggered system. The MXGS has four (adjustable) trigger windows with default settings of 300 μs , 1 ms, 3 ms, and 25 ms. When the count rate in one of these trigger windows is above a certain level of background variations, a 2-s string of data is captured and telemetered to ground. The trigger levels are set such that we receive about 100 false triggers per day. The MXGS sends a cross-trigger signal to MMIA that will also capture 2 s of data. The MMIA also triggers on a certain (adjustable) level for the digital signal of the photometers and sends a cross trigger to MXGS. This cross-trigger system allows us to capture optical signals for each TGF (observed during nighttime) and also capture MXGS measurements during all lightning and TLE events.

From launch to 1 April 2019 the two instruments have ± 80 μs relative timing accuracy and not ± 5 μs as intended. This is due to a drift term in the relative timing that varies from 0 to 160 μs and is different for every trigger. It arises due to an uncertainty in the time stamping of the MMIA photometer samples in the science data relative to the Time Correlation Pulses, which go to both instruments to ensure the relative timing accuracy, unlike MXGS where each photon is time stamped with an accuracy of ~ 1 μs relative to the Time Correlation Pulses. Fortunately, there is a register in the MMIA Data Processing Unit firmware, which can be read by the software and put into the science data to resolve the uncertainty. This required an upgrade of the onboard software and was implemented in March 2019, and after this time the relative timing accuracy is ± 5 μs for all triggered events. Before March 2019, we were able to identify the drift term for only a few events.

3. Results and Discussion

Figure 1 gives an overview of the 217 TGFs detected by ASIM during the first ten months in operation (2 June 2018 to 1 April 2019). The detection rate (Figure 1a) is about 0.7 TGF per day. This is lower than reported by other missions (RHESSI, AGILE, and Fermi) and is due to the high inclination (51.6°) of the ISS, which means that it spends more time over areas with low or no lightning activity. Figure 1b shows the geographic locations of the TGFs, which are in good agreement with earlier observations (Briggs et al., 2013; Marisaldi et al., 2014; Smith et al., 2005).

3.1. Fluence and Duration

With the verification algorithm developed for MXGS HED we can identify TGFs with less than 10 counts (Figure 2a) and duration less than 20 μs (Figure 2b). Although the fluence distribution has a maximum around 30–60 counts, there are more than 60 TGFs observed during the first 10 months with more than 100

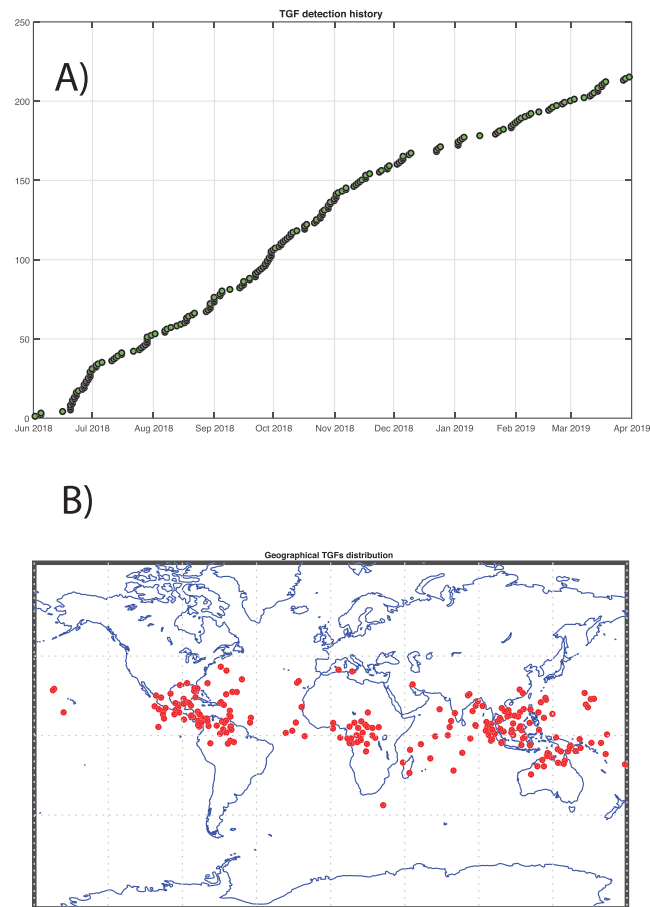


Figure 1. (a) The cumulative distribution of the observed number of TGFs versus time. (b) Geographic location of the TGFs.

counts in HED. As will be shown, ASIM has >10 times better detection capability than other missions that currently observe TGFs. This is due to two factors: (1) ASIM has a larger effective detection area and (2) ISS flies at an altitude (~ 400 km) significantly lower than the other missions.

In order to compare TGF duration with other missions, we have chosen to present the duration as t_{50} (the time from 25% to 75% of the counts) and t_{90} (the time from 5% to 95% of the counts). From Figure 2b it can be seen that t_{90} distribution has a maximum between 60 and 120 μs . The value of the t_{50} distribution has a maximum in the 20–40 μs bin and about 50% have t_{50} between 20 and 60 μs , while the t_{50} median is 45.5 μs . This is shorter than the t_{50} -maximum between 50 and 100 μs reported by Fermi when observing photons >300 keV (Connaughton et al., 2013), which is the same energy range we have used. It should be mentioned that they reported a subset of TGFs with World Wide Lightning Location Network (WWLLN) matches, which were found to be among the shorter part of the distribution. For a larger distribution of TGF (423) (not only WWLLN matches) Briggs et al. (2013) reported t_{50} and t_{90} maxima at 100–150 and 150–300 μs , respectively. Due to the better detection capability of ASIM we are able to present a more complete distribution of TGF duration, and the result indicates that TGFs are in general shorter than previously reported from space observations. For very strong and short TGFs, the MXGS HED will be saturated, which means that we miss counts in the middle of the TGF, and the t_{50} will be overestimated. Consequently, the t_{50} distribution could have a maximum even shorter than shown here. Our t_{50} distribution is consistent with the t_{50} maximum in the 0–50 μs bin reported by Marisaldi et al. (2015), but our median value of 45.5 μs is significantly shorter than their value of 86 μs . Both Marisaldi et al. (2014) and Briggs et al. (2013) recognized that their measurements were limited by instrumental dead time and that the TGF duration distribution most likely should extend to shorter timescales. From ground-based observations of high-energy photons associated with lightning strokes it has been reported durations from ~ 300 μs (Dwyer et al., 2004; Hare et al., 2016) down to six <2 μs pulses over 16 μs (Tran et al., 2015) and <10 μs pulses for hundreds of microseconds

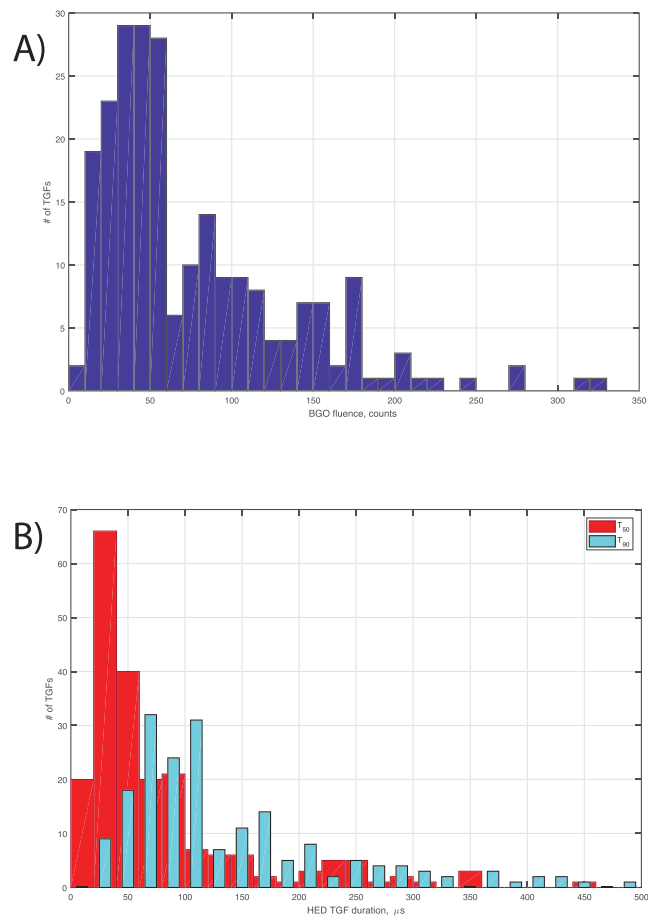


Figure 2. (a) Fluence distribution of TGF (in bins of 10 counts). (b) Duration of TGFs from the HED data defined as t_{50} and t_{90} in 20 μ s bins.

(Abbasi et al., 2018). We emphasize that our comparison with other TGF duration distributions only applies to observations from space.

3.2. The First Unique Observations by ASIM

During its first 10 months in operation ASIM has already provided what can be termed “ASIM firsts.” This is partly due to the better detection capability of MXGS and its imaging capability, but, more importantly, the simultaneous measurements of gamma rays from TGF and optical signals from lightning and TLEs.

3.2.1. Simultaneous TGF Observation From Two Platforms

Already after 20 days in operation, on 21 June 2018, ASIM MXGS HED and Fermi Gamma-ray Burst Monitor (GBM) detected the same TGF over central Africa. Simultaneous measurements of the same TGFs have previously been reported (Gjesteland et al., 2016) but never published due to the very low counting statistics. The event we report here has good counting statistics in both Fermi GBM BGO and ASIM MXGS HED and is shown in Figure 3. As can be seen in the Fermi GBM BGO measurements (Figures 3c and 3d) only the last pulse with 13 counts passed their verification algorithm and could be classified as TGF. A lightning stroke detected by the WWLLN was observed 13 μ s before this TGF was detected by Fermi. However, when lined up with the ASIM data (Figures 3a and 3b), the six counts in the Fermi GBM BGO detectors \sim 2 ms earlier were also part of a pulsed TGF. For these two pulses ASIM detected 138 and 130 counts, respectively, and also revealed at least three smaller pulses in between. The last “double” pulse detected by ASIM MXGS HED at $t = 0$ is only one pulse. The count rate is too high for HED to detect all the photons, and it is missing counts in the middle of the pulse. For the entire TGF event ASIM detected 393 counts compared with the \sim 20 detected by Fermi, a factor of 20 better detection capability. It should be mentioned that the nadir angle and distance to WWLLN location were 8° and 407 km for ASIM and 38° and 685 km for Fermi. These observations reveals that there are indeed more structures in a TGF than one would conclude from the Fermi measurements

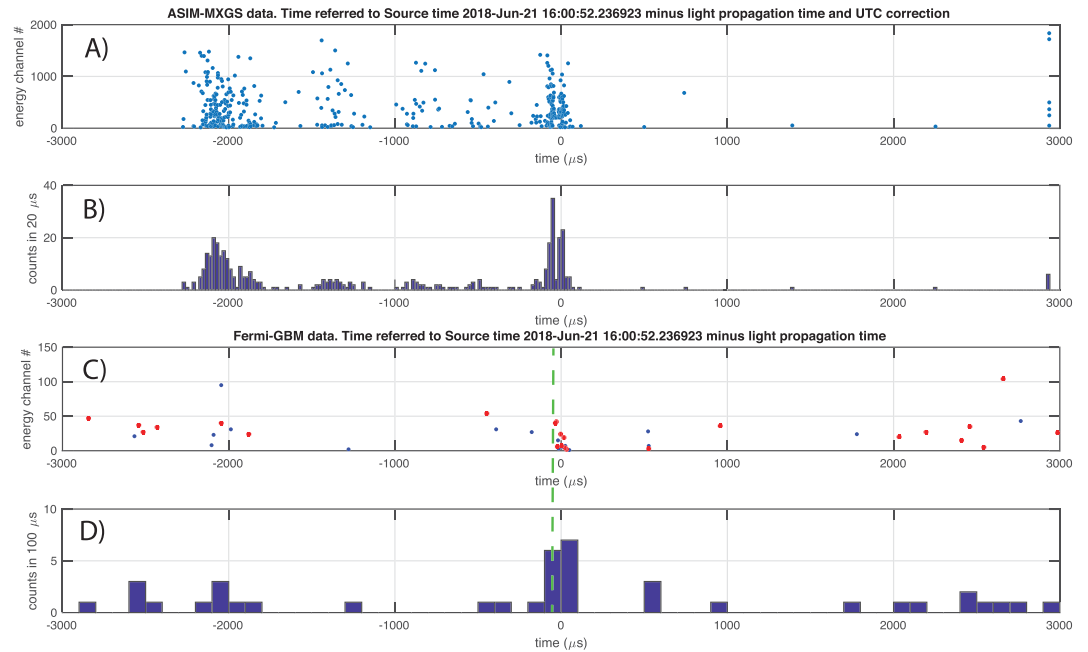


Figure 3. Simultaneous observations of a TGF over central Africa by ASIM and Fermi. (a) ADC channel versus time for MXGS HED. (b) MXGS HED counts in 20 μs bins. (c) ADC channel versus time for Fermi BGOs. Red is BGO 1 and blue BGO 2. (d) Fermi GBM BGOs counts in 100 μs bins. The green dashed line in panels (c) and (d) is the time of a lightning stroke detected by the WWLLN and was found to be simultaneous to within 13 μs of the Fermi measurements, when propagation time is accounted for.

alone. The two main pulses were 2 ms apart and the three small pulses in between were separated by 400–600 μs . This time separation could be consistent with leader steps, but it definitely indicates that there is a series of pulses. We also want to point out that the WWLLN detection was simultaneous with the last pulse, in agreement with the tendency that was reported by Mezentsev et al. (2016).

Two more simultaneous observations of TGFs from the two platforms have been identified since then (not shown), which also show large differences in detection capability. Part of this difference can be explained by ASIM MXGS BGO larger effective detection area of 650 cm^2 compared to 320 cm^2 of Fermi GBM BGO and that ISS is flying at ~ 400 km altitude while Fermi is at ~ 550 km. Other factors, like beaming direction and size of the cone angle, that can explain the differences in detected counts for these three events will be analyzed in detail in a separate paper, using all available supporting information.

3.2.2. Imaging of a TGF by ASIM

The pixelated detector layer of LED combined with the coded mask provides the imaging capability of MXGS. Figure 4 shows the imaging results for a bright TGF observed on 2 November 2018 with 316 counts in HED and 171 counts in LED (Figure 4a). We ran the imaging software with the 96 useful LED counts above channel 171 and below channel 618 (62–237 keV) in order to maximize the Tungsten pixel opacity. Figure 4b shows the imaging map of the TGF, with X and Y axes displaying the offsets with respect to the MXGS FOV center in degrees. Color scale shows Poisson Maximum Likelihood Function (MLF) defined as

$$\log \left[\frac{P(S > 0)}{P(S = 0)} \right] \quad (1)$$

where S is signal and indicates the location probability (P) on a logarithmic scale. $P(S = 0)$ is the Poisson probability for the counts “not compatible” with a given position. $P(S > 0)$ is the Poisson probability for counts compatible with a given position. In this case a unique solution was found with a MLF = 9.2. The secondary imaging artifacts have a MLF < 4.5, which is a factor of 10,000 times less probable location with respect to the solution adopted. The TGF footprint position is displayed in Figure 4c (green dot) in southern Venezuela. Lightning events from the WWLLN are indicated by the small blue and red dots. The continuous black line is the ISS position and flight direction from the center to the northeast. Figure 4d shows a more detailed map of the TGF position and lightning data restricted to 100 km \times 100 km square. With a distance to

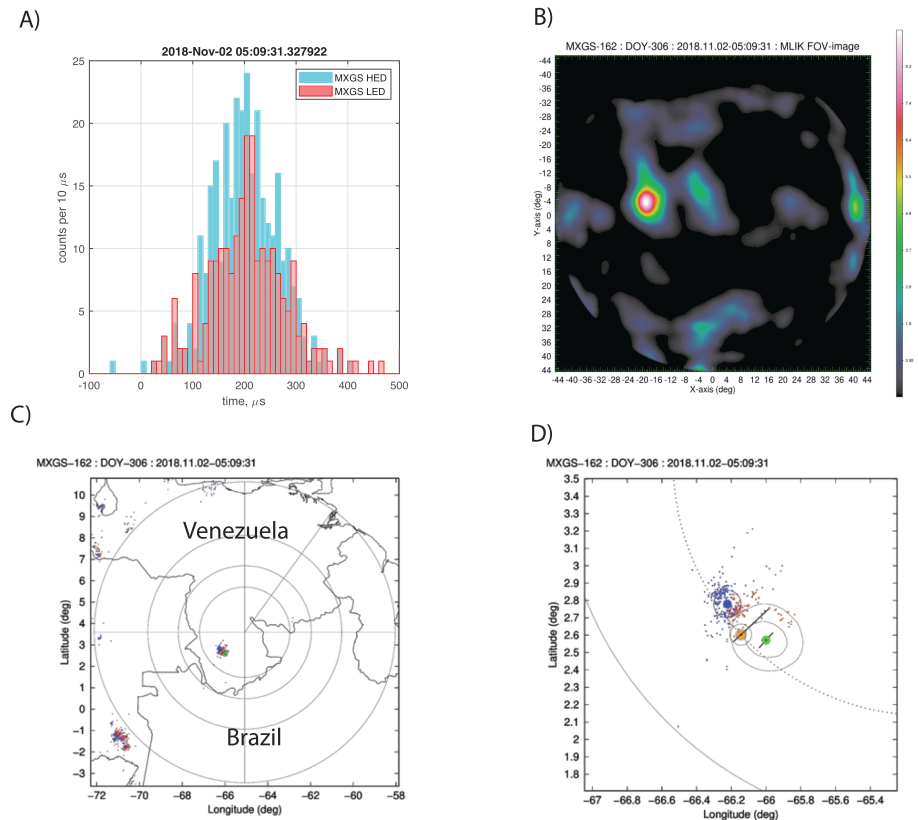


Figure 4. Imaging of a TGF observed on 2 November 2018 at 05:09:31.327922 UT over Venezuela. (a) The light curve of the TGF in HED and LED. (b) Imaging position in the FOV of the LED. (c) The position of TGF image on the map. (d) A zoomed-in view, where the green dot is the MXGS imaging position, the orange dot is the MMIA imaging position, and the small red and blue dots are the locations of the WWLLN-detected lightning activity within ± 30 min of the TGF. Red and blue dots are before and after the TGF, respectively. The large blue dot is the center of lightning activity. The small black circles indicate the one and two sigma uncertainties of the location determined by the MXGS and MMIA data, respectively.

source of 418.6 km and a source location error of 1.58° the one sigma error is 11.5 km, which is marked as the inner ellipse surrounding the TGF position. The external ellipse is the two sigma surface error radius. Blue dot is the lightning cluster center and the orange dot is the location of the lightning from the MMIA 777.4 nm camera surrounded by the error surfaces at one and two sigma. It can be seen that the two images intercept at each one's one-sigma circle. During the first 10 months of operation, we have 29 TGF observations where the count rate in LED is large enough to determine a unique TGF location, independent of other measurements of lightning activity. A dedicated paper with the first ASIM Imaging Catalogue will follow this publication.

3.2.3. TGF and Elve Produced by the Same Lightning Flash

As reported by Neubert et al. (2019a), ASIM detected for the first time that a TGF and an Elve were powered by the same lightning stroke. Here we show another clear example observed on 8 February 2019 of a TGF and an Elve produced by the same lightning stroke (Figure 5). This was a short ($\sim 40 \mu\text{s}$) but fairly bright TGF (69 and 78 counts in HED and LED, respectively; Figure 5a), where also data from the three photometers of MMIA were available. This is an event that also illustrates that, for TGFs with very high flux, the HED was missing counts in the middle of the TGF. The counts marked with yellow dots in Figure 5b are all detected on the tail of previous signals and the detector is saturated. In Figure 5c one can see an abrupt increase in all the optical channels simultaneously with the onset of the TGF (Figure 5d). While the 337 nm (blue line) and 777 nm (red line) channels show optical pulses from the lightning, the UV emissions (magenta line) are from the Elve (Neubert et al., 2019a). These emissions are excited in the ionosphere by the electromagnetic waves generated at the onset of the lightning current. It should be noted that the light curves of the lightning in the 337.0 nm and 777.4 nm (Figure 5c) are affected by scattering in the cloud implying that the rise time is not exactly the rise time of the current pulse. However, the UV emissions from the Elve should not be affected by

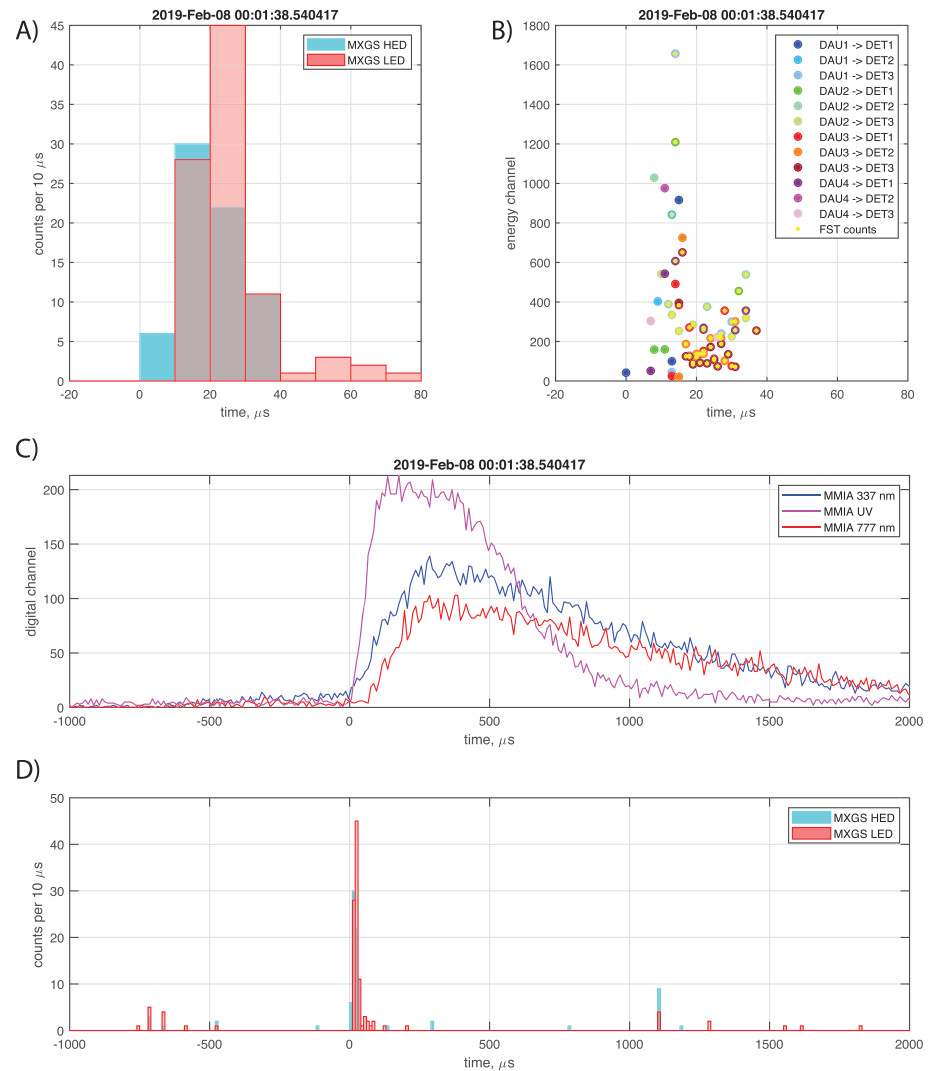


Figure 5. Simultaneous observation of a TGF and an Elve on 8 February 2019. (a) MXGS HED (light blue) and LED (red) counts in 10 μs bins. (b) ADC channel versus time for MXGS HED. Different colors indicate different BGO bars and yellow dots are signals detected at the tail of previous signal. (c) The MMIA data, where 337.0 nm is in blue, UV (180–240 nm) is in magenta, and 777.4 nm is in red. (d) Same as panel (a), but on the same time line as MMIA. The relative timing uncertainty between MXGS and MMIA, in this case, is $\pm 80 \mu\text{s}$.

scattering but will be slightly broadened due to the fast expansion of the rings in the Elve. Even though the rise times of the optical signal from the current and UV emissions excited by the electromagnetic wave can be steeper than seen by the photometers, we believe that the onsets of the signals can be determined within a few tens of microseconds. The rise time, from onset to peak, of the UV pulse is about 100 μs while the optical pulse has a rise time of 250 μs . The relative timing uncertainty between MXGS and MMIA is, in this case, $\pm 80 \mu\text{s}$. This indicates that the current pulse that generates the optical pulse has its onset simultaneous with the TGF (within the relative timing uncertainty) but develops and reaches its peak intensity after the TGF. For the case reported by Neubert et al. (2019a) it was concluded that the onset of the TGF was before the onset of the current pulse, because, in that case, the relative timing uncertainty was only $\pm 5 \mu\text{s}$ and the TGF preceded the onset of the Elve by 10 μs . Our observations are the first that support the theoretical considerations (Cummer et al., 2014; Lyu et al., 2015) and modeling predictions (Liu et al., 2017) that the lightning stroke that produces a TGF can also produce an Elve. During the first 10 months we have two simultaneous observations of TGFs and Elves to within ± 80 and $\pm 5 \mu\text{s}$, respectively, and two events where the Elve and the TGF are from the same lightning flash. We also want to point out that there is a weak

increase ~ 0.5 – 1 ms, before the TGF is produced, in the two MMIA lightning channels, which is indicative of lightning leader activity.

3.2.4. The Sequence of TGF and Main Optical Lightning Pulse

Although we can observe TGF both day and night, the photometers can only be operated during night time. Consequently, out of the 217 TGF we have observed during the first ten months, there are optical data for 94 of them. A consistent feature in a majority of these observations is that the TGF is observed during or at the end of a weak increase in the 337.0 and 777.4 nm channels, and before or at the onset of the main optical pulse. Figures 6a and 6b show the measurements from 30 June 2018 and 29 October 2018, where the onsets of TGFs are simultaneous with the onsets of the current pulses as seen by the two lightning channels. In both cases there is a weak increase in the lightning channels about 1–2 ms before the TGF. This is most pronounced in the 337.0 nm channel. We interpret this as a signature of an increased current in the leader channel probably related to the propagation of the ascending leader. However, supportive data from radio (low frequency and/or very high frequency) are needed to address this more accurately. The short TGFs (~ 150 and ~ 70 μ s) are produced just before the main 2–3 ms long optical pulses are seen. This optical pulse indicates that a large current pulse flows through the leader channel. Figure 6c shows the event on 2 November 2018, where we also see the weaker increase in the lightning channels, indicative of the propagating leader before the larger signal of a current pulse. However, in this case the TGF is produced during the leader propagation about 500 μ s before the onset of a current pulse. This TGF has a longer duration than the first two. For all these examples the relative timing uncertainty between MXGS and MMIA is ± 80 μ s.

Of the 94 TGF events where also the MMIA photometers were operated we can identify an optical pulse associated with the TGF for 58 of them with a relative timing accuracy of ± 80 μ s. For 17 events no optical pulse could be identified, most likely because the lightning stroke was outside the FOV of the photometers. There are 19 events with more than one optical pulse and more analysis and supporting data are needed to identify if any of these pulses are related to the TGF. In Figure 7 we present the distribution of the Δt between the onset of the TGF and the onset of the optical pulse for the 58 events. The onset of the TGF can be determined with a precision of about 10 μ s, while the onset of the main optical pulse is typically determined with a few tens of μ s precision. The uncertainty of the relative timing between the two onsets is therefore dominated by the relative timing uncertainty between the two instruments of ± 80 μ s. It can be seen that 49 of these 58 events (84%) cluster in a very narrow Δt distribution showing that the TGFs are produced 0–320 μ s (center of bin) ± 80 μ s before (23 events) or at (26 events) the onset of a large current pulse that flows through the leader channel. Another six TGFs (10%) have their onset up to 1 ms before the onset of the optical pulse. This is a fairly strong statistical result revealing that TGFs in general are produced just at or before the onset of a large current pulse. As shown in the three examples in Figure 6 the current pulses last for milliseconds, while the TGFs last for only a few hundred microseconds.

Like the three examples shown in Figure 6 all the 49 TGFs are seen during or at the end of a weak increase in the MMIA lightning channels starting a few milliseconds before the main current pulse. We interpret this as a signature of a propagating leader, and it implies that the leader plays an essential role in producing TGFs. As the leader propagates, the electric field ahead of the leader increases and reaches a level where it can accelerate and multiply free electrons (Babich et al., 2014, 2015; Celestin & Pasko, 2011; Moss et al., 2006) and even further by the RREA process (Gurevich et al., 1992) or in avalanche of RREAs as proposed in the feedback mechanism (Dwyer, 2008). Supportive data are needed to determine the exact production mechanism. Of these 49 TGFs, 23 are produced more than 80 μ s before the current pulse, which indicates that these are produced during the leader propagation and that the leader could still propagate after the TGF is produced, consistent with the three events reported by Cummer et al. (2015).

The large optical pulse after the TGF indicates that a large current pulse comes after the TGF, and in many cases there is only one such pulse. The optical pulse can only be the result of a large current through the leader channel. This means that the leader that produced the TGF has to connect to some conductive channels in order to make a large current pulse. Here, we will suggest two possible scenarios for this to occur. In both cases we consider that some other conductive channels have to form, either inside or out of the lower negative charge region or, inside or out of the upper positive charge region. In the first case the positive lower end of the leader will connect to the negative end of conductive channels that have formed in the lower negative charge region. In the other case the upper negative end of the leader will connect to the positive end of a conductive channel that comes down from or develops inside the upper positive charge region. To explore whether any of these scenarios really occur, one would need radio measurements (low frequency

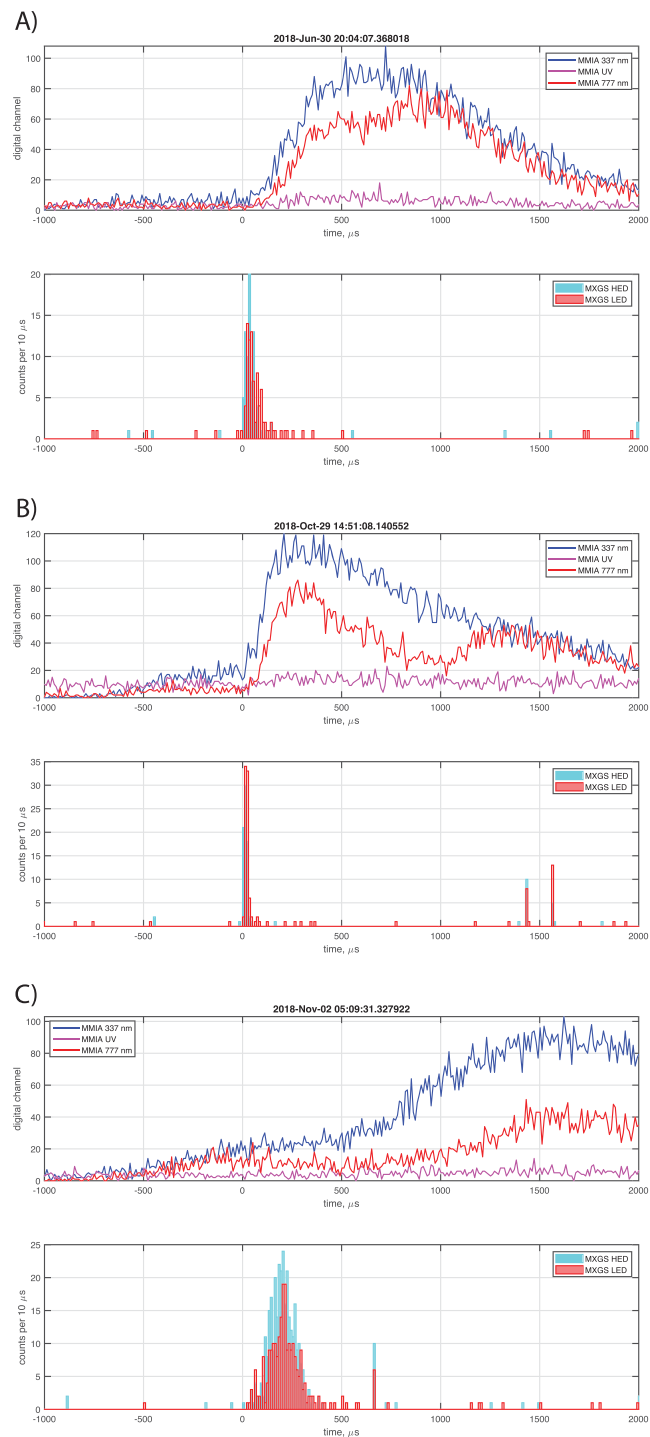


Figure 6. Three examples showing the sequence of a TGF and the optical pulses. (a) Measurements from 30 June 2018: upper panel: The MMIA data with 10 μs resolution: 337.0 nm is in blue, UV (180–240 nm) is in magenta, and 777.4 nm is in red. Lower panel: The MXGS data in 10 μs bins. HED in blue and LED in red. (b) Measurements from 29 October 2018, same format as panel (a). (c) Measurements from 2 November 2018, same format as (a). The relative timing uncertainty between MXGS and MMIA for these events is $\pm 80 \mu\text{s}$.

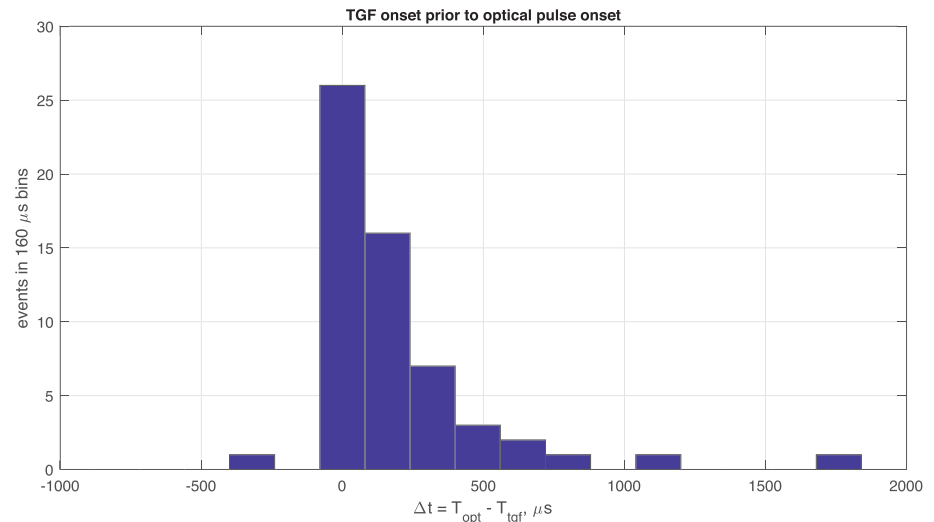


Figure 7. Distribution of Δt between the onset of the TGF and the onset of the optical pulse for 58 TGF events where the optical pulse could be identified. Bin size is 160 μs consistent with the $\pm 80 \mu\text{s}$ relative timing uncertainty between the two observations. Positive Δt means that the onset of the TGF is before the onset of the optical pulse.

and/or very high frequency), and since ASIM is just in the beginning of its mission, we foresee that we will obtain such measurements in the near future.

A few papers have reported that there is a current pulse from the TGF itself (Cummer et al., 2011; Pu et al., 2019). The current carriers in this scenario are supposed to be the secondaries produced by the relativistic electrons (Dwyer & Cummer, 2013), which means that there is no heated conductive channel involved, and we would not expect to see an optical signal from the TGF produced current. Contrary to what is seen in the majority of our events, the observations presented by Cummer et al. (2011), Lyu et al. (2015), and Pu et al. (2019) do not indicate any large current pulse after the TGF. Further investigations are needed to explore whether both a current signal from the TGF itself and a large current through the leader which makes a strong optical pulse after the TGF are common when a TGF is produced. At this point we can only state that a large current pulse that makes a strong optical pulse is seen in the majority of the TGFs observed by ASIM and that the TGFs are produced 0–320 $\mu\text{s} \pm 80 \mu\text{s}$ before the onset of the current pulse we observe.

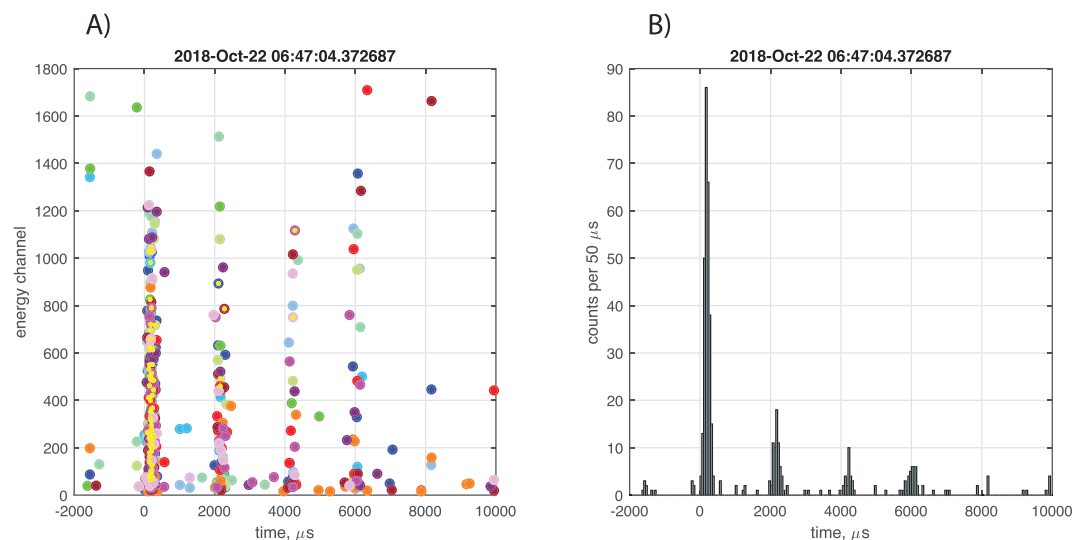


Figure 8. A multipulse TGF observed in HED on 22 October outside the West African Coast. (a) ADC channel versus time. (b) counts in 50 μs bins versus time.

3.3. Other Events

In addition to the observations presented in this paper, ASIM has detected a few Terrestrial Electron Beams with duration of several milliseconds (the first event is presented in Sarria et al., 2019) and a couple of X-ray observations from Lightning-induced Electron Precipitation. We have also detected many multipulse TGFs, typically separated by 2 ms. In Figure 8 we show one example which is almost identical to the one reported in the discovery paper by Fishman et al. (1994) (Number 1457 in their Figure 4).

4. Summary

In this paper we have presented some unprecedented observations obtained by ASIM during its first ten months in operation. These are

1. simultaneous TGFs observations by ASIM MXGS and Fermi GBM;
2. TGFs and Elves are seen from the same lightning flash;
3. the first imaging of TGFs; and
4. the sequence of TGFs and optical signals.

From these findings we can summarize the following:

1. The distribution of duration, as determined by t_{50} , has a maximum in the 20–40 μ s range and a median of 45.5 μ s, which is significantly shorter than previously reported from space observations.
2. Due to the very good detection capability of ASIM, we have identified fine structures in TGFs that cannot be seen by other missions that currently observe TGFs.
3. From 94 events where both gamma ray and optical measurements were available and with a relative timing accuracy of ± 80 μ s it is found that a majority of TGFs are produced during the upward propagation of a leader just before a large current pulse heats up the channel and emits a strong optical pulse. The onset of the TGFs precede the onset of the optical pulse by 0–320 μ s (± 80 μ s). More observations are needed to understand the system of conductive channels that are involved in order to make such a strong current pulse.

References

- Abbasi, R. U., Abu-Zayyad, T., Allen, M., Barcikowski, E., Belz, J., Bergman, D. R., et al. (2018). Gamma ray showers observed at ground level in coincidence with downward lightning leaders. *Journal of Geophysical Research: Atmospheres*, *123*, 6864–6879. <https://doi.org/10.1029/2017JD027931>
- Babich, L. P., Bochkov, E. I., & Kutsyuk, I. M. (2014). Mechanism of generation of runaway electrons in a lightning leader. *JETP Letters*, *99*(7), 386–390.
- Babich, L. P., Bochkov, E. I., Kutsyuk, I. M., Neubert, T., & Chanrion, O. (2015). A model for electric field enhancement in lightning leader tips to levels allowing X-ray and γ ray emissions. *Journal of Geophysical Research: Space Physics*, *120*, 5087–5100. <https://doi.org/10.1002/2014JA020923>
- Briggs, M. S., Fishman, G. J., Connaughton, V., Bhat, P. N., Paciasas, W. S., Preece, R. D., et al. (2010). First results on terrestrial gamma ray flashes from the Fermi Gamma-ray Burst Monitor. *Journal of Geophysical Research*, *115*, A07323. <https://doi.org/10.1029/2009JA015242>
- Briggs, M. S., Xiong, S., Connaughton, V., Tierney, D., Fitzpatrick, G., Foley, S., et al. (2013). Terrestrial gamma-ray flashes in the fermi era: Improved observations and analysis methods. *Journal of Geophysical Research: Space Physics*, *118*(6), 3805–3830. <https://doi.org/10.1002/jgra.50205>
- Celestin, S., & Pasko, V. P. (2011). Energy and fluxes of thermal runaway electrons produced by exponential growth of streamers during the stepping of lightning leaders and in transient luminous events. *Journal of Geophysical Research*, *116*, A03315. <https://doi.org/10.1029/2010JA016260>
- Chanrion, O., & Neubert, T. (2010). Production of runaway electrons by negative streamer discharge. *Journal of Geophysical Research*, *115*, A00E32. <https://doi.org/10.1029/2009JA014774>
- Chanrion, O., Neubert, T., Rasmussen, I. L., Stoltz, C., Jessen, D. T. N. C., Polny, J., et al. (2019). The Modular Multispectral Imaging Array (MMLA) of the ASIM Payload on the International Space Station. *Space Science Reviews*, *215*(4), 1–25. <https://doi.org/10.1007/s11214-019-0593-y>
- Connaughton, V., Briggs, M. S., Xiong, S., Dwyer, J. R., Hutchins, M. L., Grove, J. E., et al. (2013). Radio signals from electron beams in Terrestrial Gamma-ray Flashes. *Journal of Geophysical Research: Space Physics*, *118*, 2313–2320. <https://doi.org/10.1029/2012JA018288>
- Cummer, S. A., Briggs, M. S., Dwyer, J. R., Xiong, S., Connaughton, V., Fishman, G. J., et al. (2014). The source altitude, electric current, and intrinsic brightness of terrestrial gamma ray flashes. *Geophysical Research Letters*, *41*, 8586–8593. <https://doi.org/10.1002/2014GL062196>
- Cummer, S. A., Lu, G., Briggs, M. S., Connaughton, V., Xiong, S., Fishman, G. J., & Dwyer, J. R. (2011). The lightning-TGF relationship on microsecond timescales. *Geophysical Research Letters*, *38*, L14810. <https://doi.org/10.1029/2011GL048099>
- Cummer, S. A., Lyu, F., Briggs, M. S., Fitzpatrick, G., Roberts, O. J., & Dwyer, J. R. (2015). The lightning leader altitude progression in terrestrial gamma-ray flashes. *Geophysical Research Letters*, *42*, 7792–7798. <https://doi.org/10.1002/2015GL065228>
- Cummer, S. A., Zhai, Y., Hu, W., Smith, D. M., Lopez, L. I., & Stanley, M. A. (2005). Measurements and implications of the relationship between lightning and terrestrial gamma ray flashes. *Geophysical Research Letters*, *32*, L08811. <https://doi.org/10.1029/2005GL022778>

Acknowledgments

The data described in this paper are available from the authors on request (nikolai.ostgaard@uib.no) and can also be downloaded from the Asim Science Data Centre (ASDC) homepage after a proposal has been submitted and approved. All the data that are used to produce the figures in this paper, including a list of the 217 TGFs with time, location, duration, and counts, are uploaded to Zenodo with doi: 10.5281/zenodo.3460503. This study was supported by the European Research Council under the European Union's Seventh Framework Programme (FP7/2007-2013)/ERC Grant Agreement 320839 and the Research Council of Norway under Contracts 208028/F50 and 223252/F50 (CoE). This study has received funding from the European Union's Horizon 2020 research and innovation program under the Marie Skłodowska-Curie grant agreement SAINT 722337. ASIM is a mission of ESA's SciSpace Programme for scientific utilization of the ISS and non-ISS space exploration platforms and space environment analogues. ASIM was funded through the ESA ELIPS program, through contracts with TERMA and Danish Technical University (DTU) in Denmark, University of Bergen (UB) in Norway, and University of Valencia (UV) in Spain. Additional funding was supported by the ESA PRODEX Contracts PEA 4000105639 and 4000111397 to DTU and ESA PRODEX Contract 4000102100 and by Norwegian Research Council to UB. The ASIM Science Data Centre (ASDC) at DTU is supported by PRODEX Contract PEA 4000115884 and by PRODEX Contract PEA 4000123438 at UB. The ASIM Science Data Centre and data analysis activities at the UV are supported by the MINECO Research Grants ESP2015-69909-C5-1-R and ESP2017-86263-C4-1-R.

- Dwyer, J. R. (2008). Source mechanisms of terrestrial gamma-ray flashes. *Journal of Geophysical Research*, *113*, D10103. <https://doi.org/10.1029/2007JD009248>
- Dwyer, J. R., & Cummer, S. (2013). Radio emissions from terrestrial gamma-ray flashes. *Journal of Geophysical Research: Space Physics*, *118*, 3769–3790. <https://doi.org/10.1002/jgra.50188>
- Dwyer, J. R., Rassoul, H. K., Al-Dayeh, M., Caraway, L., Wright, B., Chrest, A., et al. (2004). A ground level gamma-ray burst observed in association with rocket-triggered lightning. *Geophysical Research Letters*, *31*, L05119. <https://doi.org/10.1029/2003GL018771>
- Dwyer, J. R., & Smith, D. M. (2005). A comparison between Monte Carlo simulations of runaway breakdown and terrestrial gamma-ray flash observations. *Geophysical Research Letters*, *32*, L22804. <https://doi.org/10.1029/2005GL023848>
- Fishman, G. J., Baht, P. N., Mallozzi, R., Horack, J. M., Koshut, T., Kouveliotou, C., et al. (1994). Discovery of intense gamma-ray flashes of atmospheric origin. *Science*, *164*, 1313.
- Gjesteland, T., Østgaard, N., Bitzer, P., & Christian, H. J. (2017). On the timing between Terrestrial Gamma ray Flashes, radio atmospheric and optical lightning emission. *Journal of Geophysical Research: Space Physics*, *122*, 7734–7741. <https://doi.org/10.1002/2017JA024285>
- Gjesteland, T., Østgaard, N., Smith, D., Briggs, M. S., & Marisaldi, M. (2016). Stereo observations of terrestrial gamma-ray flashes. European Geosciences Union General Assembly Abstracts, EGU2016-11968.
- Gjesteland, T., Østgaard, N., Stadsnes, J., Connell, P. H., & Fishman, G. J. (2010). Effects of deadtime losses on terrestrial gamma ray flash measurements done by the Burst And Transient Source Experiment. *Journal of Geophysical Research*, *115*, A00E21. <https://doi.org/10.1029/2009JA014754>
- Gurevich, A. V., Milikh, G. M., & Roussel-Dupré, R. (1992). Runaway electron mechanism of air breakdown and preconditioning during a thunderstorm. *Physics Letters A*, *165*(5-6), 463–468. [https://doi.org/10.1016/0375-9601\(92\)90348-P](https://doi.org/10.1016/0375-9601(92)90348-P)
- Hare, B. M., Uman, M. A., Dwyer, J. R., Jordan, D., Biggerstaff, M. I., Caicedo, J. A., et al. (2016). Ground-level observation of a terrestrial gamma ray flash initiated by a triggered lightning. *Journal of Geophysical Research: Atmospheres*, *121*, 6511–6533. <https://doi.org/10.1002/2015JD024426>
- Liu, N., Dwyer, J. R., & Cummer, S. A. (2017). Elves accompanying terrestrial gamma ray flashes. *Journal of Geophysical Research: Space Physics*, *122*, 10,563–10,576. <https://doi.org/10.1002/2017JA024344>
- Lu, G., Blakeslee, R. J., Li, J., Smith, D. M., Shao, X.-M., McCaul, E. W., et al. (2010). Lightning mapping observation of a terrestrial gamma-ray flash. *Geophysical Research Letters*, *37*, L11806. <https://doi.org/10.1029/2010GL043494>
- Lyu, F., Cummer, S. A., & McTague, L. (2015). Insights into high peak current in-cloud lightning events during thunderstorms. *Geophysical Research Letters*, *42*, 6836–6843. <https://doi.org/10.1002/2015GL065047>
- Marisaldi, M., Argan, A., Urzi, A., Gjesteland, T., Fuschino, F., Labanti, C., et al. (2015). Enhanced detection of terrestrial gamma-ray flashes by AGILE. *Geophysical Research Letters*, *42*, 9481–9487. <https://doi.org/10.1002/2015GL066100>
- Marisaldi, M., Fuschino, F., Labanti, C., Galli, M., Longo, F., Monte, E. D., et al. (2010). Detection of terrestrial gamma ray flashes up to 40 MeV by the AGILE satellite. *Journal of Geophysical Research*, *107*, A00E13. <https://doi.org/10.1029/2009JA014502>
- Marisaldi, M., Fuschino, F., Tavani, M., Dietrich, S., Price, C., Galli, M., et al. (2014). Properties of terrestrial gamma ray flashes detected by AGILE MCAL below 30 MeV. *Journal of Geophysical Research: Space Physics*, *119*, 1337–1355. <https://doi.org/10.1002/2013JA019301>
- Marisaldi, M., Galli, M., Labanti, C., Østgaard, N., Sarria, D., Cummer, S. A., et al. (2019). On the high-energy spectral component and fine time structure of terrestrial gamma-ray flashes. *Journal of Geophysical Research: Atmospheres*, *124*, 7484–7497. <https://doi.org/10.1029/2019JD030554>
- Mezentsev, A., Østgaard, N., Gjesteland, T., Albrechtsen, K., Lehtinen, N., Marisaldi, M., et al. (2016). Radio emissions from double RHESSI TGFs. *Journal of Geophysical Research: Atmospheres*, *121*, 8006–8022. <https://doi.org/10.1002/2016JD025111>
- Moss, G. D., Pasko, V. P., Liu, N., & Veronis, G. (2006). Monte Carlo model for analysis of thermal runaway electrons in streamer tips in transient luminous events and streamer zones of lightning leaders. *Journal of Geophysical Research*, *111*, A02307. <https://doi.org/10.1029/2005JA011350>
- Neubert, T., Østgaard, N., Reglero, V., Blanc, E., Chanrion, O., Oxborrow, C. A., et al. (2019b). The ASIM Mission on the International Space Station. *Space Science Reviews*, *215*(2), 26. <https://doi.org/10.1007/s11214-019-0592-z>
- Neubert, T., Østgaard, N., Reglero, V., Chanrion, O., Heumesser, M., Dimitriadou, K., et al. (2019a). *A Terrestrial Gamma-ray Flash and Ionospheric UV Emissions Powered by a Lightning Discharge*. *215*(2), 1–7. <https://doi.org/10.1126/science.aax3872>
- Østgaard, N., Balling, J. E., Bjørnsen, T., Brauer, P., Budtz-Jørgensen, C., Bujwan, W., et al. (2019). The Modular X- and Gamma-Ray Sensor (MXGS) of the ASIM payload on the International Space Station. *Space Science Reviews*, *215*(2), 28. <https://doi.org/10.1007/s11214-018-0573-7>
- Østgaard, N., Gjesteland, T., Carlson, B. E., Collier, A. B., Cummer, S. A., Lu, G., & Christian, H. J. (2013). Simultaneous observations of optical lightning and terrestrial gamma ray flash from space. *Geophysical Research Letters*, *40*, 2423–2426. <https://doi.org/10.1002/grl.50466>
- Pu, Z., Cummer, S. A., Lyu, F., Briggs, M., Mailyan, B., Stanbro, M., & Roberts, O. (2019). Low frequency radio pulses produced by terrestrial gamma-ray flashes. *Geophysical Research Letters*, *46*, 6990–6997. <https://doi.org/10.1029/2019GL082743>
- Sarria, D., Kochkin, P., Østgaard, N., Lehtinen, N., Mezentsev, A., Carlson, M. B., et al. (2019). The first terrestrial electron beam observed by The atmosphere-space interactions monitor. *Journal of Geophysical Research: Space Physics*, *124*, 1–15. <https://doi.org/10.1029/2019JA027071>
- Shao, X. M., Hamlin, T., & Smith, D. M. (2010). A closer examination of terrestrial gamma-ray flash-related lightning processes. *Journal of Geophysical Research*, *115*, A00E30. <https://doi.org/10.1029/2009JA014835>
- Skeltved, A. B., Østgaard, N., N. Lehtinen, Mezentsev, A., & Carlson, B. (2017). Constraints to do realistic modeling of the electric field ahead of the tip of a lightning leader. *Journal of Geophysical Research: Atmospheres*, *122*, 8120–8134. <https://doi.org/10.1002/2016JD026206>
- Smith, D. M., Lopez, L. L., Lin, R. P., & Barrington-Leigh, C. P. (2005). Terrestrial gamma-ray flashes observed up to 20 MeV. *Science*, *307*, 1085–1088.
- Stanley, M. A., Shao, X. M., Smith, D. M., Lopez, L. I., Pongratz, M. B., Harlin, J. D., et al. (2006). A link between terrestrial gamma-ray flashes and intracloud lightning discharges. *Geophysical Research Letters*, *33*, L06803. <https://doi.org/10.1029/2005GL025537>
- Tran, M. D., Rakov, V. A., Mallick, S., Dwyer, J. R., Nag, A., & Heckman, S. (2015). A terrestrial gamma-ray flash recorded at the Lightning Observatory in Gainesville, Florida. *Journal of Atmospheric and Solar-Terrestrial Physics*, *136*, 86–93. <https://doi.org/10.1016/j.jastp.2015.10.010>
- Wilson, C. T. R. (1925). The acceleration of β -particle in strong electrical fields of thunderclouds. *Proceedings of the Cambridge Philosophical Society*, *22*, 534–538.